Contrib Mineral Petrol (1997) 126: 292–302 

V. López Sánchez-Vizcaíno · J. A. D. Connolly
M. T. Gómez-Pugnaire

# Metamorphism and phase relations in carbonate rocks from the Nevado-Filábride Complex (Cordilleras Béticas, Spain): application of the Ttn + Rt + Cal + Qtz + Gr buffer

Received: 11 October 1995 / Accepted 5 August 1996

**Abstract** Phase relations and metamorphic conditions have been studied in metacarbonate rocks from the Nevado-Filábride Complex (Cordilleras Béticas) through forward modeling. In many rock samples, the assemblage titanite + rutile + calcite + quartz + graphite buffered the composition of the C-O-H fluid present during metamorphism. Over a wide range of *P-T* conditions, fluid compositions computed for this buffer are essentially binary $H_2O$-$CO_2$ mixtures. This buffer also constrains the chemical potentials of $TiO_2$, CaO and $SiO_2$. Consequently it is possible to make a thermodynamic projection through these components to predict the stable phase relations consistent with the buffer. Using this method, phase relations have been analyzed in a rock containing the buffer assemblage and paragonite, albite, phengite, epidote, and chlorite. The equilibrium *P-T* conditions for this assemblage are constrained, by minimization of the differences between predicted and observed mineral compositions, to be 560 ± 15 °C and 9.5 ± 1 kbar. Conditions obtained compare well with those estimated from other studies in different lithologic units. The inferred metamorphic fluid composition is $H_2O$-rich ($X_{CO_2} < 0.2$).

V. López Sánchez-Vizcaíno (✉)
Departamento de Geología, Universidad de Jaén,
Escuela Universitaria Politécnica,
Calle Alfonso X el Sabio 28, E-23700
Linares, Spain

J.A.D. Connolly
Institut für Mineralogie und Petrographie,
ETH Zentrum, Sonneggstrasse 5,
CH-8092 Zürich, Switzerland

M.T. Gómez-Pugnaire
Departamento de Mineralogía y Petrología,
Universidad de Granada, Avda Fuentenueva s/n,
E-18002 Granada, Spain

Editorial responsibility: V. Trommsdorff

## Introduction

The complexity of thermobarometry in impure metacarbonate rocks from a regional metamorphism accounts for the paucity of temperature (*T*) and pressure (*P*) data for such rocks (Hewitt 1973; Franz and Spear 1983; Ganguin 1986; Castelli 1991; Ballèvre and Lagabrielle 1994). The complexity is a consequence of the high variance of most assemblages present in these lithologies. Because of such complications with metacarbonate parageneses, in the Nevado-Filábride (Cordilleras Béticas, Spain) past workers have concluded that the intermediate to high-pressure event reported in other rocks (metabasites and metapelites) was not recorded by the carbonates (Nijhuis 1964; Voet 1967; Gómez-Pugnaire 1979; Vissers 1981; Martínez-Martínez 1984; Jabaloy 1991). In this paper it is shown that the high variance of such assemblages is sometimes illusory, and, when this is so, forward modeling can be used to establish that relatively high *P* conditions are recorded by these rocks in the Nevado-Filábride Complex.

Forward modeling is often complicated by the high variance of the major mineral assemblages. However, accessory minerals may determine (i.e., buffer) the chemical potentials of one or more components as a function of pressure and temperature (Korzhinskii 1959). While this has been recognized for some time, many potentially useful buffers appear to have been overlooked. This paper reports an application of such a buffer, the assemblage Ttn + Rt + Cal + Qtz + Gr (notation after Kretz 1983), in the analysis of phase relations of metacarbonate rocks from the Nevado-Filábride Complex. Given the assumption that the assemblage Ttn + Rt + Cal + Qtz + Gr equilibrated in the presence of a C-O-H fluid, this buffer determines the chemical potentials of 6 components ($CO_2$, $H_2O$, $O_2$, CaO, $SiO_2$ and $TiO_2$) as a function of *P* and *T*. Phase relations for the metacarbonates can then be simplified by thermodynamic projection into the $K_2O$-$Na_2O$-$Al_2O_3$-FeO-MgO subcomposition, from which it is subsequently possible to establish the physicochemical conditions of metamorphism by forward modeling of mineral solution behavior.

## Geological setting

Metacarbonate rocks from the Nevado-Filábride Complex of the Cordilleras Béticas (Fig. 1) have been studied in the central part of the Sierra de los Filabres, in the area bounded by the villages of Macael and Cóbdar (Fig. 2). The Cordilleras Béticas, located in the western Mediterranean and continued to the south in the Rif Chain (North Africa), are formed by two domains of continental crust: Sudiberic Domain, and Alborán Domain (Fig. 1). The Nevado-Filábride Complex is the lowermost tectonic unit of the Alborán Domain (Balanyá and García-Dueñas 1986).

The Nevado-Filábride Complex consists of two main lithological sequences (Fig. 1). The lower one, probably prePermian, is composed of graphitic pelites, quartzites and marbles, and minor intercalated metagranite bodies (Brouwer 1926). The upper, Permo-Triassic or younger, sequence (Nijhuis 1964) is made up of metapelites, metapsammites, marbles and calc-schists at the top, and relatively small metabasite and serpentinite bodies (Brouwer 1926). The sedimentation environment of these upper rocks has been deduced as shallow marine deposited on materials of continental affinity (Gómez-Pugnaire et al. 1994; López Sánchez-Vizcaíno et al. 1995).

The upper sequence was strongly deformed and metamorphosed during the Alpine Orogeny, although the majority of the present structures are related to a late extensional episode that obliterated most of the previous structures (Jabaloy 1991). An earlier compressional event is deduced from the general structural configuration of the complex in several superposed tectonic units, and from the presence of relict structures (transposed fold hinges) and high-pressure metamorphic parageneses (particularly in metapelites and metabasites, Gómez-Pugnaire 1979). The Alpine metamorphism evolved from the high-pressure event ($P$ = 9–20 kbar, $T$ = 350–690 °C) (Gómez-Pugnaire 1979; Gómez-Pugnaire and Fernández-Soler 1987; Bakker et al. 1989; Puga et al. 1989; Gómez-Pugnaire et al. 1994), through amphibolite facies conditions ($P$ = 6–8 kbar, $T$ = 550–610 °C) (Puga and Díaz de Federico 1976; Gómez-Pugnaire 1979; Gómez-Pugnaire and Fernández-Soler 1987; Bakker et al. 1989), to a final low-pressure and low-temperature episode ($P$ < 5 kbar, $T$ = 340–425 °C) (Gómez-Pugnaire and Fernández-Soler 1987; Bakker et al. 1989).

This work concerns the marbles and calc-schists of the upper sequence of the Macael-Cóbdar zone. In this area (Fig. 2) metacarbonate rocks appear at the top of two minor tectonic units, which also comprise a thick pelitic-psammitic sequence (Tahal Formation), a fine-grained pelitic sequence of evaporitic origin (Gómez-Pugnaire et al. 1994) and a basement of dark prePermian rocks. At the contact between the carbonate and pelitic sequences, intrusive basalt and gabbro bodies are common (Voet 1967).

The marble and calc-schist sequence (Voet 1967; López Sánchez-Vizcaíno 1994) consists (Fig. 2b) of a heterogeneous series of pure, locally brecciated, calcite and dolomite marbles, calc-schists, metapelites, quartzites, and minor serpentinite and metabasite bodies. Within this series, further subdivision is not possible as there are only two stratigraphic markers: a pure gray calcite marble with boudins of centimeter-size black graphitic carbonate, and impure marbles and calc-schists with chromium-rich silicates and heavy minerals (López Sánchez-Vizcaíno 1994; López Sánchez-Vizcaíno et al. 1995). Intercalations of graphitic rocks (carbonate-bearing and pelitic) are common through the entire series, the carbonate-bearing ones being the subject of this work.

## Petrography

The mineralogy of impure marbles and calc-schists is comprised of albite, amphibole, calcite, chlorite, dolomite, epidote group minerals, garnet, muscovite, paragonite, phlogopite and quartz, with apatite, chalcopyrite, graphite, pyrite, titanite, tourmaline, and rutile as accessory minerals.

There is no systematic variation of the mineralogy in the field and metamorphic zones cannot be established. This is common in all lithological units of the Nevado-Filábride Complex and may be,

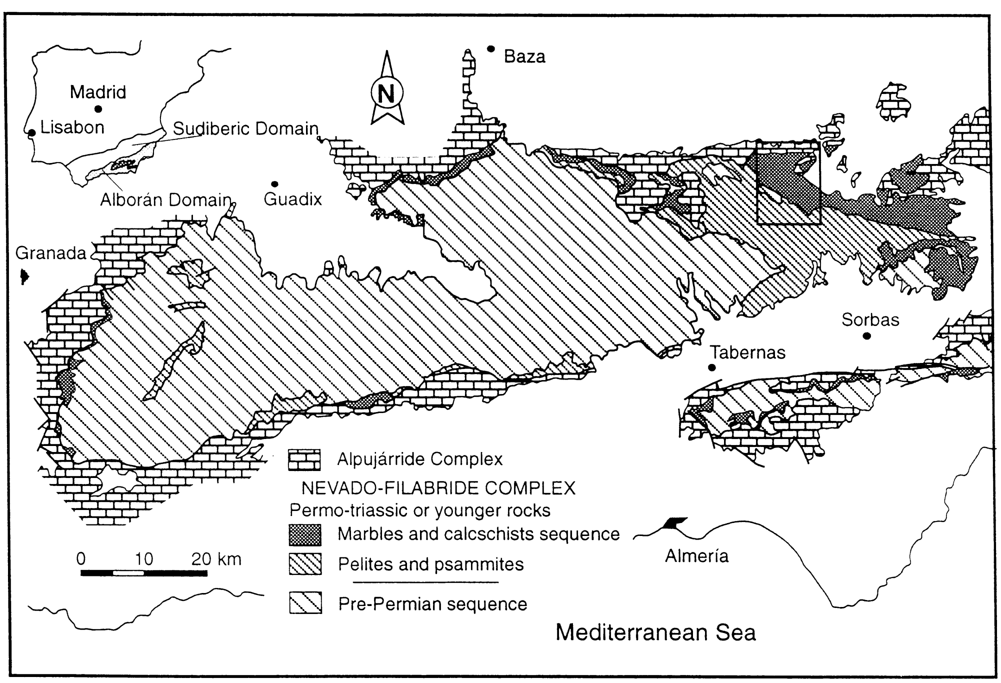


**Fig. 1** Geological map of Nevado-Filábride Complex of the Cordilleras, Betic as showing distribution of prePermian and Permo-Triassic or younger materials

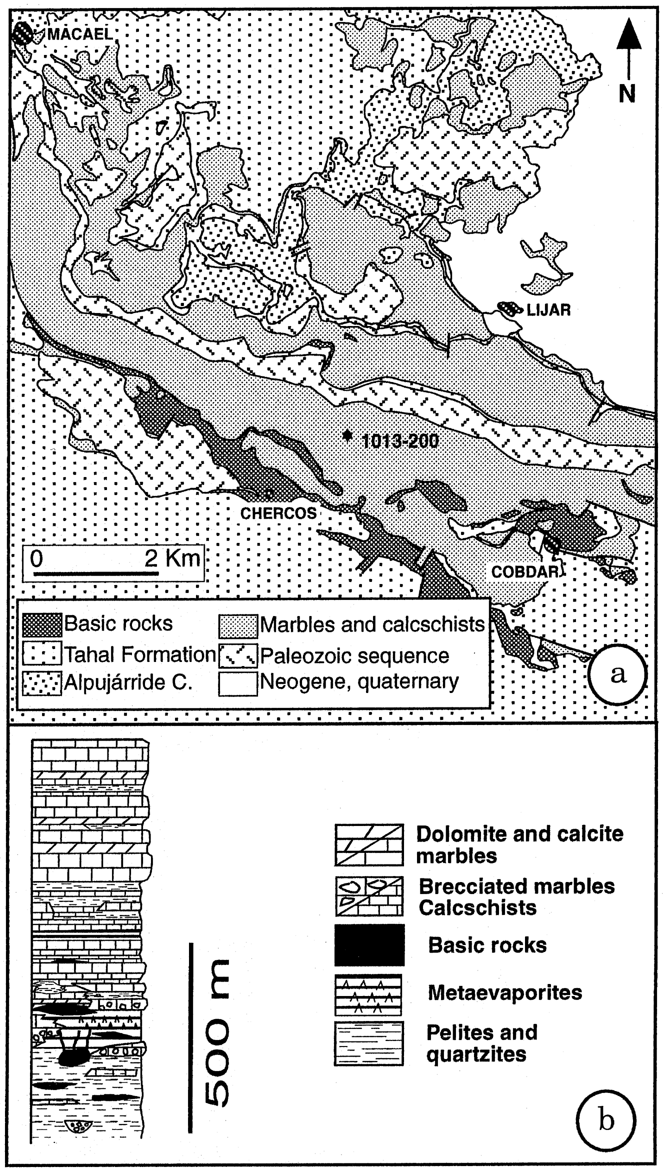


**Fig. 2 a** Geological map of the Macael-Cóbdar area with location of sample 1013–200. **b** Column showing stratigraphy of Permo-Triassic rocks in this area

at least in part, related to the complicated postmetamorphic tectonic evolution.

The most characteristic fabric in many samples is a penetrative planar structure correlatable to the regional main foliation. This foliation is marked by muscovite, amphibole, epidote minerals, titanite and deformed carbonate grains. In muscovite-rich samples, a later crenulation also appears and has induced rotation of epidote and titanite grains. There is sporadic evidence for an earlier deformation from a foliation, sometimes crenulated, within zoisite, titanite and garnet porphyroblasts. The least pelitic carbonate rocks have a massive fabric and the relationships between growth and deformation are difficult to establish. Taking these uncertainties into account, some conclusions concerning mineral growth-deformation relationships in these rocks can be deduced:

1. Minerals such as muscovite, amphibole and garnet have grown over long periods of time, both before and after the formation of the main foliation.

2. Epidote group minerals appear as large zoisite and clinozoisite porphyroblasts prior to the main foliation, but most clinozoisite is synkinematic.

3. Prograde phlogopite and chlorite appear as isolated aggregates, or in equilibrium with each other and with other minerals (muscovite and titanite) in massive rocks. Neither habit can be correlated with any planar fabric. Chlorite and phlogopite also occur as retrograde minerals replacing epidote, garnet, and amphibole.

4. Paragonite forms fine-grained aggregates, frequently intergrown with muscovite, prior to the main foliation.

5. Albite is found in two different textural contexts: as idiomorphic postkinematic crystals, or as rounded xenomorphic grains with ambiguous relationships to other phases.

6. Titanite has crystallized in all stages and appears both oriented parallel to the main foliation and as inclusions in prekinematic porphyroblasts of garnet and clinozoisite. Coexisting titanite and rutile are observed in many cases and rutile is rarely found alone.

7. Graphite is present in almost every lithologic unit, though more abundantly in mineralogically simple marbles. There are few differences in mineralogy between graphite-bearing and graphite-absent rocks, e.g., epidote, which is more common in non-graphitic units.

The metamorphic evolution of the carbonate rocks and its correlation with other well-known lithologies of the Nevado-Filábride Complex is difficult to establish from textural relationships, due to the long crystallization period of most of the important phases. This implies that they have recorded changing environmental conditions during metamorphism. Only three mineral reactions are clearly preserved in the studied metacarbonate rocks:

amphibole + epidote = chlorite + calcite + quartz

epidote = plagioclase + calcite

titanite = rutile + calcite + quartz

These reactions do not always occur and in most samples there is no textural evidence of these specific reactions.

## Mineral chemistry

Mineral chemistries were analyzed with an automated Cameca SX50 electron microprobe at ETH Zürich. Routine measurement conditions for silicates were 15 kV acceleration voltage, and 20 nA beam current. Carbonate analyses were done at 15 kV acceleration voltage, and 6 nA beam current. Natural and synthetic oxides and silicates were used for standardization. Unless otherwise noted minerals are homogeneous within a given sample and show no significant zoning. No notable differences exist between mineral compositions in graphitic and non-graphitic rocks.

### Albite

Plagioclase is albitic with < 10% anorthite.

### Amphibole

Amphiboles show a complex chemical composition. Following Leake (1978), they can be classified as calcic (Mg-hornblende and actinolitic hornblende) or sodic-calcic (barroisite), although there is a compositional transition from one to another type. This composition can be described, following Thompson (1981), by the additive component tremolite and the following exchange vectors: $Al_2Mg_{-1}Si_{-1}$ (tschermakite), $NaSiCa_{-1}Al_{-1}$ (plagioclase), and $NaAlSi_{-1}$ (edenite). Halogen contents are low.

### Biotite

Most biotite analyses (Table 1) are phlogopite rich ($X_{Mg}$ = 0.6–0.8). The $^{VI}Al$ values vary between 0.003 and 0.54 atoms per formula unit (p.f.u.), and Ti contents are low (0.03–0.16 p.f.u.). The F-content is 0.732–3.49 wt%, and Cl-content is 0.019–0.18 wt%.

### Carbonates

Calcite and dolomite are nearly stoichiometric in most cases. Molecular $MgCO_3 + FeCO_3$ in calcite is < 10 mol%. In dolomite the $FeCO_3$ is < 10%.

### Chlorite

Chlorite analyses (Table 1) have homogeneous values for tschermakitic and dioctahedral substitutions, related to petrographic association. A stronger variation appears in $X_{Mg}$ (0.49–0.82).

### Epidote group minerals

Epidote group minerals display a wide chemical variation between the end-members $Ca_2Al_3Si_3O_{12}(OH)$ and $Ca_2Al_2FeSi_3O_{12}(OH)$ (Table 1; Fig. 3). Clinozoisite is both more abundant and iron rich than zoisite.

Although there is no homogeneous zonation in clinozoisite, there is a tendency for Fe-enrichment toward grain cores with a maximum variation of 2–3% $Fe_2O_3$. Minor compositional changes also appear at contacts with other minerals. These complex zonation patterns are similar to those described by Franz and Selverstone (1992) for Fe-rich clinozoisites.

### Garnet

Garnet contains <66 mol% almandine, with high grossular contents (19–33%), minor pyrope (2.6–11.9%) and strongly variable spessartine (2.3–22.28%), usually < 12% (Fig. 4).

### Muscovite

Muscovite analyses show considerable variation (Table 2): Si (3.026–3.4), $^{VI}Al$ (1.374–1.94), Mg (0.066–0.405), Fe (0–0.257), Na (0.040–0.511), K (0.382–0.892). The Ti and halogen contents are low (<0.53% $TiO_2$, <0.56% F, <0.05% Cl). Some of the compositional extremes are from an almost stoichiometric muscovite found in one sample. In most other samples, muscovite is phengitic with wide $X_{Mg}$ variation related, at least in part, to changes in rock bulk composition and to paragenetic association.

### Paragonite

Paragonite shows little chemical variation (Table 2), except for high K-contents (up to 0.35 p.f.u) in some grains that may reflect the presence of fine-grained muscovite intergrowths.

### Titanite

The titanite analyses have always more than 85% of the $CaTiSiO_5$ end-member (Table 2). The Al (<6% $Al_2O_3$), F (<1.92% F) and $Fe^{3+}$ (<3.83% $Fe_2O_3$) components are present in most of the cases. The main substitution mechanism explaining this is

$$Ti + O = (Al, Fe^{3+}) + (OH, F) \text{ (Fig. 5)},$$

with F/(F + OH) = 0.25–1. The high Al and F may be related to high *P-T* conditions (Franz and Spear 1985; Enami et al. 1993), but the rock bulk composition may also have influence, as shown by high $Fe_2O_3$ contents that are correlatable with high $Fe_2O_3$ values in epidote.

## Phase relations and metamorphic conditions

In conventional geo-thermobarometry observed mineral compositions are assumed to be those of a relict phase equilibrium. These compositions are then used to make adjustments to idealized end-member equilibria to reconstruct the physicochemical conditions of metamorphism. An alternative approach is applied here in which thermodynamic modeling is used to predict the compositional variation of the mineralogy as a function of physicochemical conditions. A match is then sought between the observed and predicted mineral compositions. The advantage of this "forward modeling" (Connolly et al. 1994) approach is that the analysis provides a test for the consistency of the thermodynamic models used for the mineral solution behavior and the observed mineralogy.

In the Nevado-Filábride Complex, the metacarbonate and calc-schist phase equilibria are complicated by the large number of compositional degrees of freedom in both individual minerals and in the fluid phase that is presumed to have coexisted with these minerals. Often such complications preclude rigorous thermodynamic analysis; however, the presence of additional minerals with simple, or fixed, stoichiometries in the metacarbonates and calc-schists implies that the system has few compositional degrees of freedom. This restriction can be expressed through a component saturation hierarchy (Connolly 1990) that determines the chemical potentials of the saturated components solely as a function of pressure and temperature. In contrast to earlier applications of this method, here a component saturation hierarchy is used to constrain the composition and chemical potentials of a C-O-H fluid as well as various mineral solutions.

**Table 1** Representative analyses and formulas of biotite, chlorite and epidote.

| Mineral | Biotite | | | | Chlorite | | | | Epidote | | | | |
|---|---|---|---|---|---|---|---|---|---|---|---|---|---|
| Sample | 21B–28 | 21B–28 | 1013–163 | 1013–36 | 1013–200 | 1013–122 | 1013–16 | 1013–21 | 1013–122 | 1013–200 | 22V–1 | 25C–29 | 1013–3 |
| $SiO_2$ | 40.43 | 40.40 | 41.43 | 39.43 | 25.59 | 25.37 | 27.97 | 26.47 | 37.60 | 37.76 | 39.61 | 39.05 | 37.99 |
| $TiO_2$ | 0.33 | 0.50 | 0.44 | 0.66 | 0.08 | 0.06 | 0.01 | 0.05 | 0.20 | 0.17 | 0.05 | 0.03 | 0.12 |
| $Al_2O_3$ | 15.17 | 14.73 | 13.70 | 15.85 | 22.24 | 21.17 | 20.88 | 20.57 | 27.87 | 23.42 | 32.90 | 32.29 | 23.37 |
| $Cr_2O_3$ | 0.05 | 0.05 | 0.00 | 0.00 | 0.02 | 0.00 | 2.19 | 0.03 | 0.04 | 0.01 | 0.03 | 0.33 | 1.18 |
| $Fe_2O_3$ | – | – | – | – | – | – | – | – | 8.47 | 13.65 | 1.17 | 1.40 | 12.46 |
| FeO | 10.50 | 10.29 | 9.08 | 13.86 | 22.65 | 22.25 | 12.57 | 20.15 | – | – | – | – | – |
| MgO | 19.21 | 19.18 | 20.31 | 15.81 | 17.45 | 17.67 | 24.58 | 19.90 | 0.02 | 0.00 | 0.03 | 0.03 | 0.00 |
| MnO | 0.01 | 0.01 | 0.02 | 0.00 | 0.05 | 0.05 | 0.07 | 0.04 | 0.10 | 0.06 | 0.02 | 0.00 | 0.26 |
| CaO | 0.06 | 0.07 | 0.00 | 0.06 | 0.19 | 0.03 | 0.07 | 0.01 | 23.77 | 23.40 | 24.70 | 24.60 | 23.03 |
| $Na_2O$ | 0.24 | 0.17 | 0.18 | 0.14 | 0.04 | 0.00 | 0.02 | 0.00 | 0.01 | 0.01 | 0.00 | 0.02 | 0.02 |
| $K_2O$ | 9.16 | 9.21 | 9.46 | 8.72 | 0.03 | 0.00 | 0.00 | 0.00 | 0.01 | 0.02 | 0.00 | 0.00 | 0.01 |
| F | 2.64 | 2.81 | 2.98 | 0.92 | 0.00 | 0.00 | 0.00 | 0.00 | 0.00 | 0.00 | 0.00 | 0.00 | 0.00 |
| Cl | 0.08 | 0.13 | 0.02 | 0.12 | 0.02 | 0.00 | 0.00 | 0.00 | 0.00 | 0.00 | 0.00 | 0.00 | 0.00 |
| | Cations per 11 oxygens | | | | Cations per 28 oxygens | | | | Cations per12 oxygens and 1 OH–group | | | | |
| Total | 97.88 | 97.55 | 97.61 | 95.58 | 88.35 | 86.66 | 88.36 | 87.22 | 98.09 | 98.50 | 98.51 | 97.75 | 98.44 |
| O = Cl,F | 1.15 | 1.24 | 1.26 | 0.44 | 0.00 | 0.00 | 0.00 | 0.00 | 0.00 | 0.00 | 0.00 | 0.00 | 0.00 |
| Total | 96.73 | 96.31 | 96.35 | 95.14 | 88.35 | 86.66 | 88.36 | 87.22 | 98.09 | 98.50 | 98.51 | 97.75 | 98.44 |
| Si | 2.947 | 2.965 | 3.028 | 2.943 | 5.270 | 5.330 | 5.490 | 5.451 | 2.937 | 2.992 | 2.995 | 2.983 | 3.008 |
| $^{IV}Al$ | 1.053 | 1.035 | 0.972 | 1.057 | 2.730 | 2.670 | 2.510 | 2.549 | – | – | – | – | – |
| $^{VI}Al$ | 0.251 | 0.240 | 0.208 | 0.338 | 2.670 | 2.570 | 2.310 | 2.443 | 2.566 | 2.186 | 2.931 | 2.907 | 2.181 |
| Ti | 0.018 | 0.028 | 0.024 | 0.037 | 0.010 | 0.010 | 0.000 | 0.008 | 0.012 | 0.010 | 0.003 | 0.002 | 0.007 |
| Cr | 0.003 | 0.003 | 0.000 | 0.000 | 0.000 | 0.000 | 0.340 | 0.005 | 0.002 | 0.001 | 0.002 | 0.020 | 0.074 |
| $Fe^{3+}$ | – | – | – | – | – | – | – | – | 0.498 | 0.814 | 0.066 | 0.080 | 0.742 |
| $Fe^{2+}$ | 0.636 | 0.627 | 0.550 | 0.857 | 3.900 | 3.910 | 2.060 | 3.470 | – | – | – | – | – |
| Mg | 2.087 | 2.098 | 2.212 | 1.759 | 5.360 | 5.530 | 7.190 | 6.109 | 0.003 | 0.000 | 0.003 | 0.004 | 0.000 |
| Mn | 0.001 | 0.001 | 0.001 | 0.000 | 0.010 | 0.010 | 0.010 | 0.007 | 0.006 | 0.004 | 0.001 | 0.000 | 0.017 |
| Ca | 0.005 | 0.006 | 0.000 | 0.004 | 0.040 | 0.010 | 0.010 | 0.002 | 1.990 | 1.986 | 2.001 | 2.013 | 1.954 |
| Na | 0.034 | 0.024 | 0.026 | 0.021 | 0.020 | 0.000 | 0.010 | 0.000 | 0.001 | 0.002 | 0.000 | 0.003 | 0.003 |
| K | 0.852 | 0.862 | 0.882 | 0.831 | 0.010 | 0.000 | 0.000 | 0.000 | 0.001 | 0.002 | 0.001 | 0.000 | 0.001 |
| F | 0.967 | 1.028 | 1.087 | 0.335 | 0.000 | 0.000 | 0.000 | 0.000 | 0.000 | 0.000 | 0.000 | 0.000 | 0.000 |
| Cl | 0.016 | 0.025 | 0.004 | 0.024 | 0.010 | 0.000 | 0.000 | 0.000 | 0.000 | 0.000 | 0.000 | 0.000 | 0.000 |

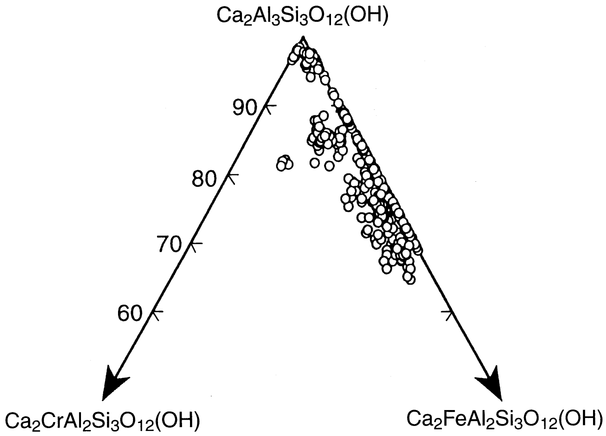


**Fig. 3** Chemical variation of epidote minerals, zoisite and clinozoisite between the end-members $Ca_2Al_3Si_3O_{12}(OH)$, $Ca_2CrAl_2Si_3O_{12}(OH)$ and $Ca_2FeAl_2Si_3O_{12}(OH)$. See also López Sánchez-Vizcaíno et al. (1995)

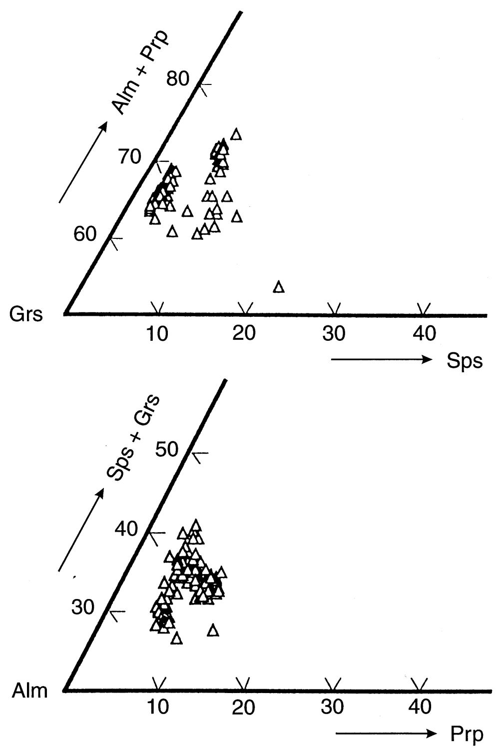


**Fig. 4** Garnet compositions for Alm, Prp, Grs and Sps components

## Phase relations in graphitic rocks: the Ttn-Rt-Cal-Qtz-Gr buffer

The paragenesis titanite-rutile-calcite-quartz has been recognized as an important buffer of $CO_2$-$H_2O$ fluids (Ernst 1972; Hunt and Kerrick 1977; Nesbitt and Essene 1983) through the equilibrium:

$$\mathrm{Rt + Cal + Qtz = Ttn + CO_2} \tag{1}$$

If graphite is also present with the other minerals, as is often the case in metacarbonates and calc-schists of the Nevado-Filábride Complex, equilibrium (1) can be combined with:

$$\mathrm{CO_2 = Gr + O_2} \tag{2}$$

to formulate a buffer for oxygen chemical potential or fugacity:

$$\mathrm{Rt + Cal + Qtz = Ttn + Gr + O_2} \tag{3}$$

Given the reasonable assumptions that the relevant minerals have compositions essentially in the CaO-$TiO_2$-$SiO_2$ system, and that a C-O-H fluid phase coexisted with these minerals at lithostatic pressure, equilibrium (3) implies that fluid composition, and the partial molar Gibbs energy of any fluid species, are uniquely determined as a function of pressure and temperature. These properties were computed using the HSMRK (Kerrick and Jacobs 1981) and MRK (Holloway 1977) equations of state as described elsewhere (Connolly 1995). Figure 6 shows the bulk composition, after projection through carbon, and oxygen fugacity for a C-O-H fluid buffered by equilibrium (3) as a function of pressure and temperature. The bulk composition of the fluid (Fig. 6a) is defined by the variable $X_O$, which expresses the atomic fraction of oxygen relative to oxygen + hydrogen [i.e., $X_O = n_O/(n_O + n_H)$]. Because the $f_{O_2}$ of the Rt-Cal-Qtz-Ttn-Gr buffer is relatively oxidizing (Fig. 6b), the fluid is nearly a binary $H_2O$-$CO_2$ mixture (e.g., see Fig. 2 of Connolly 1995), and the mole fractions of these species can be approximated, with an accuracy of better than 1 mol%, as $y_{CO_2} = 1 - y_{H_2O} = (3X_O - 1)/(X_O + 1)$ (Connolly 1995). In Fig. 6a it can be seen that equilibrium (3) is stable over a wide range of *P-T* conditions and that the bulk fluid composition is always more oxidized than the $X_O$ = 1/3 composition at which water activity is a maximum; thus the abundance of methane and other reduced species is negligible except at low temperatures when the fluid composition approaches the $X_O$ = 1/3 composition (Connolly 1995). As shown in Fig. 7 equilibrium (3) defines an isobarically univariant curve in an isobaric $T$-$X_O$ section, which is analogous to the locus of equilibrium (1) in conventional isobaric $T$-$X_{CO_2}$ diagrams. The high-temperature extremum of the isobaric equilibrium at $X_O$ = 1 in Fig. 7 corresponds to the maximum thermal stability of the buffer assemblage shown in Fig. 6.

The utility of the buffer described by equilibrium (3) is magnified by the fact that it constrains the chemical potentials of CaO, $TiO_2$, and $SiO_2$, as well as those of the volatile components. Accordingly it is possible to make a thermodynamic projection through these components so as to eliminate them from the thermodynamic composition space that must be considered for the analysis of phase relations. In practice this is done with a computer program (available upon request from the second author, Connolly 1990), that determines identities and compositions of the stable phases in the saturated component space (CaO-$SiO_2$-$TiO_2$-C-O-H) at each *P-T* condition of interest. The stable phase rela-

**Table 2** Representative analyses and formulas of muscovite, chlorite and epidote.

| Mineral | Muscovite | | | | Paragonite | | | Titanite | | | | |
|---|---|---|---|---|---|---|---|---|---|---|---|---|
| Sample | 1013–200 | 21B–19 | 21B–28 | 1013–123 | 1013–122 | 1013–200 | 1013–200 | 1013–122 | 1013–122 | 1013–163 | 1013–200 | 1013–200 |
| $SiO_2$ | 49.11 | 48.28 | 49.39 | 49.97 | 47.09 | 47.32 | 47.37 | 30.54 | 29.95 | 30.83 | 30.55 | 30.58 |
| $TiO_2$ | 0.29 | 0.33 | 0.25 | 0.16 | 0.17 | 0.07 | 0.12 | 34.36 | 37.65 | 31.22 | 36.04 | 35.17 |
| $Al_2O_3$ | 28.56 | 30.68 | 29.36 | 27.40 | 39.66 | 39.20 | 38.67 | 4.49 | 2.42 | 5.80 | 2.61 | 3.07 |
| $Cr_2O_3$ | 0.02 | 0.05 | 0.00 | 0.00 | 0.02 | 0.03 | 0.05 | 0.07 | 0.00 | 0.00 | 0.00 | 0.00 |
| $Fe_2O_3$ | – | – | – | – | – | – | – | 0.00 | 0.21 | 0.64 | 0.63 | 0.80 |
| FeO | 3.54 | 1.41 | 1.53 | 1.88 | 0.93 | 0.85 | 0.89 | 0.29 | 0.00 | 0.00 | 0.00 | 0.00 |
| MgO | 2.52 | 2.80 | 3.29 | 3.25 | 0.01 | 0.05 | 0.00 | 0.11 | 0.00 | 0.00 | 0.00 | 0.01 |
| MnO | 0.00 | 0.00 | 0.00 | 0.01 | 0.45 | 0.10 | 0.12 | 0.02 | 0.03 | 0.00 | 0.03 | 0.00 |
| CaO | 0.07 | 0.17 | 0.02 | 0.00 | 0.38 | 0.22 | 0.20 | 27.31 | 29.02 | 29.02 | 29.13 | 28.81 |
| $Na_2O$ | 0.78 | 0.96 | 0.73 | 0.57 | 6.61 | 7.11 | 6.93 | 0.06 | 0.07 | 0.00 | 0.04 | 0.05 |
| $K_2O$ | 10.38 | 9.49 | 9.99 | 10.04 | 1.31 | 0.70 | 0.91 | 0.51 | 0.02 | 0.00 | 0.00 | 0.01 |
| F | 0.00 | 0.14 | 0.54 | 0.22 | 0.00 | 0.00 | 0.00 | 0.00 | 0.00 | 1.92 | 0.94 | 1.07 |
| Cl | 0.01 | 0.05 | 0.03 | 0.01 | 0.00 | 0.00 | 0.00 | 0.00 | 0.00 | 0.00 | 0.00 | 0.00 |
| | Cations per 11 oxygens | | | | Cations per 11 oxygens | | | Cations calculated after Franz and Spear (1985) | | | | |
| Total | 95.28 | 94.36 | 95.13 | 93.51 | 96.64 | 95.65 | 95.26 | 97.76 | 99.37 | 99.42 | 99.97 | 99.57 |
| O = F,Cl | 0.00 | 0.07 | 0.23 | 0.09 | 0.00 | 0.00 | 0.00 | 0.00 | 0.00 | 0.81 | 0.40 | 0.45 |
| Total | 95.28 | 94.29 | 94.90 | 93.42 | 96.64 | 95.65 | 95.26 | 97.76 | 99.37 | 98.61 | 99.57 | 99.12 |
| Si | 3.307 | 3.241 | 3.306 | 3.393 | 2.983 | 3.017 | 3.033 | 0.994 | 0.970 | 0.997 | 0.991 | 0.995 |
| $^{IV}Al$ | 0.693 | 0.759 | 0.694 | 0.607 | 1.018 | 0.984 | 0.967 | – | – | – | – | – |
| $^{VI}Al$ | 1.574 | 1.668 | 1.622 | 1.586 | 1.943 | 1.962 | 1.952 | 0.172 | 0.092 | 0.221 | 0.879 | 0.860 |
| Ti | 0.015 | 0.017 | 0.013 | 0.008 | 0.008 | 0.003 | 0.006 | 0.841 | 0.917 | 0.760 | 0.100 | 0.118 |
| Cr | 0.001 | 0.003 | 0.000 | 0.000 | 0.001 | 0.002 | 0.003 | 0.002 | 0.000 | 0.000 | 0.000 | 0.000 |
| $Fe^{3+}$ | – | – | – | – | – | – | – | 0.000 | 0.005 | 0.015 | 0.016 | 0.020 |
| $Fe^{2+}$ | 0.199 | 0.079 | 0.085 | 0.107 | 0.049 | 0.045 | 0.048 | 0.008 | 0.000 | 0.000 | 0.000 | 0.000 |
| Mg | 0.253 | 0.281 | 0.328 | 0.329 | 0.042 | 0.010 | 0.012 | 0.006 | 0.000 | 0.000 | 0.000 | 0.001 |
| Mn | 0.000 | 0.000 | 0.000 | 0.001 | 0.001 | 0.003 | 0.000 | 0.001 | 0.001 | 0.000 | 0.001 | 0.000 |
| Ca | 0.005 | 0.012 | 0.002 | 0.000 | 0.026 | 0.015 | 0.014 | 0.952 | 1.007 | 1.006 | 1.012 | 1.004 |
| Na | 0.102 | 0.125 | 0.095 | 0.075 | 0.812 | 0.879 | 0.860 | 0.004 | 0.005 | 0.000 | 0.003 | 0.003 |
| K | 0.891 | 0.813 | 0.853 | 0.870 | 0.106 | 0.057 | 0.074 | 0.021 | 0.001 | 0.000 | 0.000 | 0.000 |
| F | 0.002 | 0.061 | 0.229 | 0.094 | 0.000 | 0.000 | 0.000 | 0.000 | 0.000 | 0.196 | 0.096 | 0.110 |
| Cl | 0.003 | 0.011 | 0.006 | 0.002 | 0.000 | 0.000 | 0.000 | 0.000 | 0.000 | 0.000 | 0.000 | 0.000 |

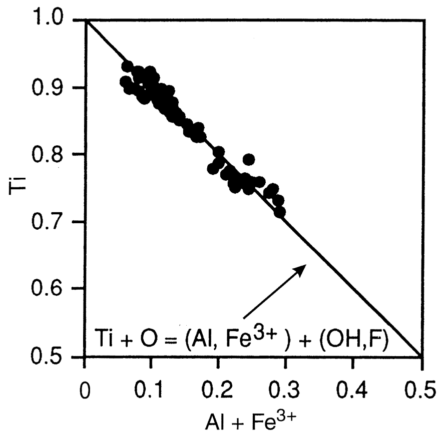


**Fig. 5** Chemical variation of titanite as described by the Ti + O = (Al, $Fe^{3+}$) + (OH, F) substitution

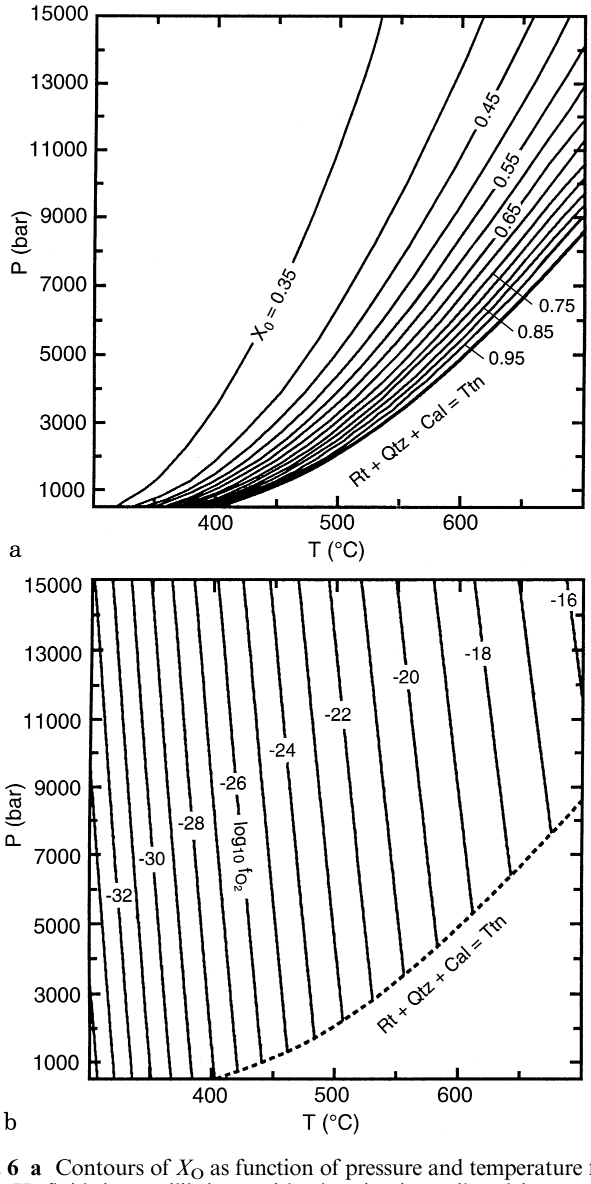


**Fig. 6 a** Contours of $X_O$ as function of pressure and temperature for C-O-H fluid in equilibrium with the titanite-rutile-calcite-quartz-graphite buffer (contour interval is 0.05 mole). **b** Variation of $\log_{10} f_{O_2}$, contoured at one log unit intervals, for the same fluid as in **a**

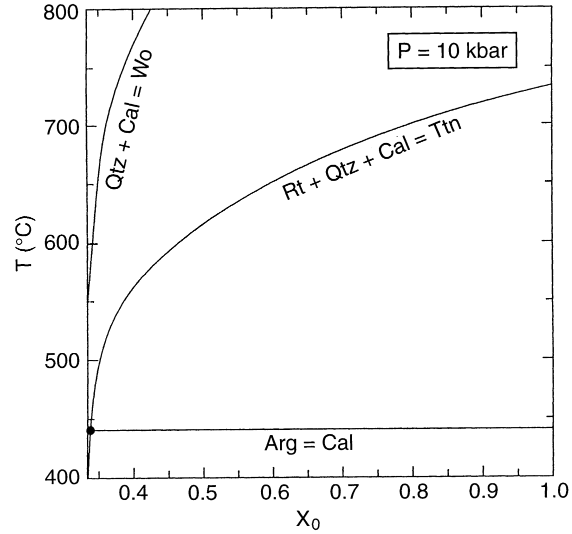


**Fig. 7** Isobaric $T$-$X_O$ diagram, for the CaO-$SiO_2$-$TiO_2$-C-O-H system, showing conditions for the stability of the titanite-rutile-calcite-quartz-graphite buffer. The stability field of calcite is limited by wollastonite and aragonite stability

tions consistent with these phases are then determined as a function of the remaining compositional variables (here, those defining the $K_2O$-$Na_2O$-$Al_2O_3$-FeO-MgO composition space). For this purpose, thermodynamic mineral data were taken from a revised version (Holland 1994, personal communication) of Holland and Powell's (1990) database.

## Sample 1013–200

Phase relations have been calculated for a graphite-saturated rock (sample 1013–200) in which the mineral association Ttn-Rt-Qtz-Cal-Gr buffered the fluid composition. Phase notation, and the mineralogy and mineral chemistry of this sample are given in Table 3 and Table 4 respectively.

The minerals can be represented in the system $SiO_2$-$Al_2O_3$-CaO-$Na_2O$-$K_2O$-Fe-MgO-$TiO_2$-C-O-H. In addition to the observed minerals (Table 4), dolomite and the solid solution tremolite-ferrotremolite, not found in the

**Table 3** Phase notation and formulas used in $P$-$T$ diagram (Fig. 8)

| Notation | Phase | Formula |
|---|---|---|
| $Ab_x$ | Albite | $Na_xCa_{1-x}Al_{2-x}Si_{2+x}O_8$ |
| $Cal_x$ | Calcite | $Ca_xMg_{1-x}(CO_3)_{2-x}$ |
| $Chl_{x-y}$ | Chlorite | $Mg_{5x}Fe_{5(1-x)}Al_{4+2y}Si_{3-y}O_{10}(OH)_8$ |
| dol | Stoichiometric dolomite | $CaMg(CO_3)_2$ |
| $Ep_x$ | Epidote | $Ca_2Al_{3-x}Fe_xSi_3O_{12}(OH)$ |
| $Pa_x$ | Paragonite | $Na_xK_{1-x}Al_3Si_3O_{10}(OH)_2$ |
| $Phen_{x-y}$ | Phengite | $KMg_xFe_yAl_{3-2(x+y)}Si_{3+x+y}$ $O_{10}(OH)_2$ |
| Rt | Stoichiometric rutile | $TiO_2$ |
| $Tr_x$ | Tremolite | $Ca_2Mg_{5x}Fe_{5(1-x)}Si_8O_{22}(OH)_2$ |
| Ttn | Stoichiometric titanite | $CaTiSiO_5$ |

**Table 4** Comparison of observed and predicted mineral compositions for sample 1013–200 (at *P-T* conditions in the *center* of the *shaded field* of Fig. 8). Phase notation as in Table 3. Mixing properties of mineral solutions have been taken from Newton et al. (1980) (albite-anorthite), Berman (1990) (garnet), and Chatterjee and Froese (1975) (muscovite-paragonite). The remaining solid solutions (epidote, chlorite, tremolite and phengite) were modeled as ideal, assuming site populations as in Holland and Powell (1990).

| Minerals | Observed composition | Predicted composition |
|---|---|---|
| Albite | $Ab_{96}$–$Ab_{91}$ | $Ab_{91}$ |
| Calcite | $Cc_{90}$–$Cc_{100}$ | $Cc_{100}$ |
| Chlorite | $Chl_{56-63}$–$Chl_{60-71}$ | $Chl_{48-77}$–$Chl_{60-81}$ |
| Dolomite | – | dol |
| Epidote | $Ep_{65}$–$Ep_{90}$ | $Ep_{35}$ |
| Paragonite | $Pa_{88}$–$Pa_{94}$ | $Pa_{85}$–$Pa_{90}$ |
| Phengite | $Phen_{7-16}$–$Phen_{13-4}$ | $Phen_{7.5-15}$ |
| Rutile | Rt | Rt |
| Titanite | Ttn | Ttn |
| Tremolite | – | $Tr_{10}$–$Tr_{18}$ |

rock, were included in the calculations. The stability fields of these phases define boundaries for the stability conditions of the observed parageneses.

After projection through O, $TiO_2$, CaO and $SiO_2$, phase relations can be represented in the $Na_2O$-$K_2O$-$Al_2O_3$-FeO-MgO subsystem as a function of *P* and *T*. Projection through O accounts for both iron-oxidation states. The stability field of the observed paragenesis, paragonite + chlorite + phengite + albite + epidote, is limited by the equilibria (Fig. 8):

$$\mathrm{Pa + Tr = Ab + Chl + Ep + Phen} \tag{4}$$

and

$$\mathrm{Chl + Pa = Phen + Ab + Ep + dol} \tag{5}$$

The stable phases at pressures higher and temperatures lower than (4) and temperatures higher than (5) are tremolite and dolomite, respectively. Both reaction (4) and (5) intersect at an invariant point at 10900 bar and 583 °C. The predicted mineral compositions for the paragonite + chlorite + phengite + albite + epidote paragenesis are shown in Fig. 8b–f. In each diagram the thin (dashed or solid) curves correspond to isopleths for the specified mineral.

Within the paragonite + chlorite + phengite + albite + epidote stability field, both the Na-content of plagioclase (Fig. 8b) and the Fe-content of epidote (Fig. 8c) decrease with temperature and increase with pressure. The muscovite component of paragonite also increases with temperature (Fig. 8d). Chlorite becomes richer in Mg (thin solid lines) with temperature, and poorer in Tschermaks component (hatched lines) with *P* (Fig. 8e).

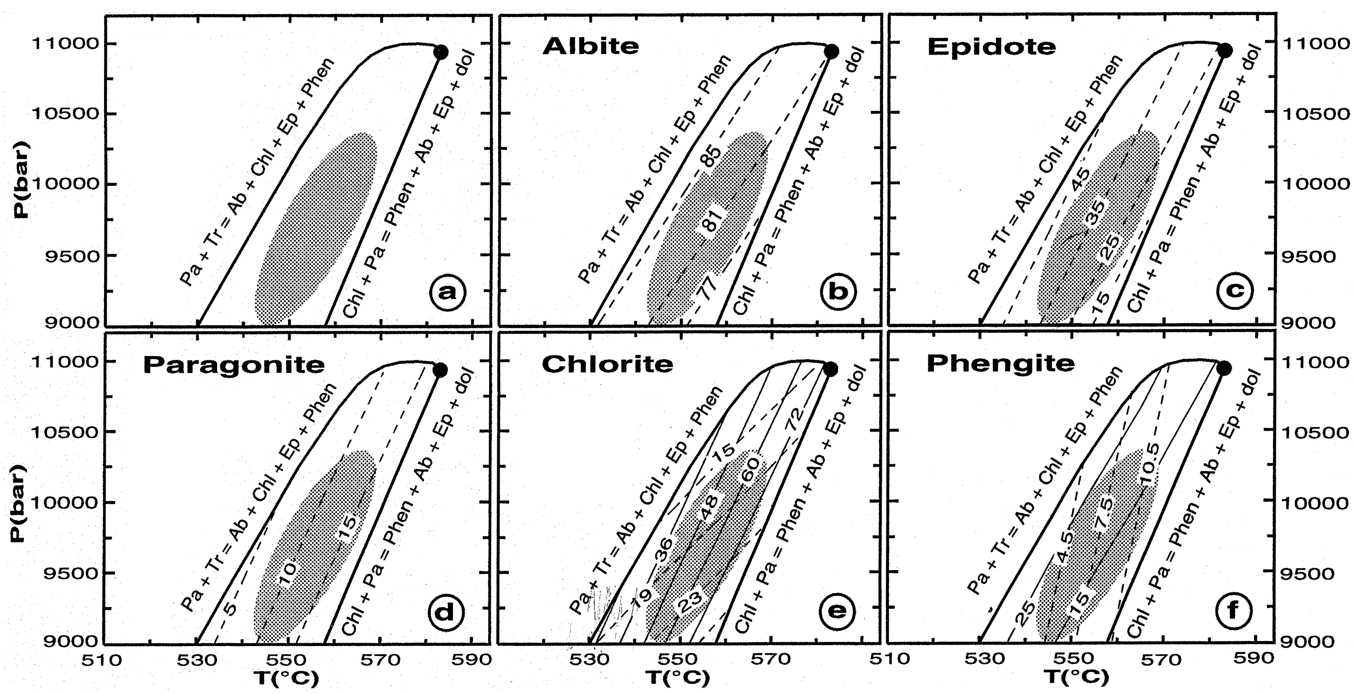


**Fig. 8a–f** *P-T* projection calculated for sample 1013–200 in the system $Al_2O_3$-$Na_2O$-$K_2O$-MgO-Fe, after projection through O, $TiO_2$, CaO and $SiO_2$. Phase notation and definition of isopleths as in Table 3. **a** Calculated stability field; *solid thick curves* represent univariant equilibria (see text) limiting the stability field of the paragonite + chlorite + phengite + albite + epidote paragenesis. The *filled dot* represents the invariant point at which univariant equilibria intersect. The *shaded field* represents *P-T* conditions where discrepancies between the predicted and observed compositions are minimized. **b** Albite ($X_{Ab}$) isopleths. **c** Epidote ($X_{Al_2Fe}$) isopleths (Fe-content in epidote decreases with *T* and increases with *P*). **d** Paragonite ($X_{Na}$) isopleths. **e** Chlorite isopleths; *solid thin lines* contour $X_{Mg}$ in chlorite and *dashed lines* contour Tschermaks substitution in chlorite. **f** Phengite isopleths; *dashed lines* contour celadonite content in phengite and *thin solid lines* contour ferroceladonite content in phengite

Increasing temperature, or decreasing pressure, favors the Tschermaks substitution in phengite (Fig. 8f).

The conditions for equilibrium of the paragonite + chlorite + phengite + albite + epidote paragenesis in sample 1013–200, the shaded region of Fig. 8, were estimated to be 9.5 ± 1 kbar and 560 ± 15 °C. This estimate was obtained by minimizing the differences between the observed and predicted mineral compositions (Table 4). In the calculations, calcite and rutile were treated as pure phases. This matches well with their actual compositions. The observed composition of titanite contains up to 16% of $CaAlSiO_4$(F, OH); however, no thermodynamic data are available for this end-member of the solid solution, and it has been also considered a pure phase. Calculations done with the titanite activity model of Ghent and Stout (1994) indicate that the Al-solution in titanite causes only small differences (*P* is 350 bar higher at 550 °C) in the equilibrium conditions for reaction (1). These differences become negligible at $H_2O$-rich conditions, such as are implicit in the present analysis (Fig. 7).

The largest discrepancies between observed and predicted compositions occur in epidote (Fig. 8c). The predicted composition of epidote in the center of the shaded area is richer in the clinozoisite component ($Ep_{35}$) than that observed in the rock ($Ep_{65–90}$). This difference is probably due to the inadequacy of the ideal solution model used here. The agreement between predicted and observed compositions of the remaining minerals (albite, paragonite, chlorite and phengite) is relatively good, with a maximum discrepancy of <15 mol% at the edge of the shaded field (Table 4 and Fig. 8b, d, e and f).

Factors controlling the uncertainties for the predicted conditions: thermodynamic data for end-member phase components, solution models, and the dependence of the stability field of the phases from other phases of the system, are discussed in detail in Connolly et al. (1994).

### Fluid phase composition

Oxygen fugacity ($f_{O_2}$) and fluid phase composition ($X_O$) were calculated for sample 1013–200 in the *P-T* field where the mineral assemblage is predicted to be stable. The values obtained are very homogeneous: $\log f_{O_2}$ varies between −19.0 and −21.2 and $X_O$ = 0.36–0.41 (see Fig. 6). The metamorphic fluid phase was therefore a $H_2O$-rich fluid with $y_{CO_2}$ = 0.07–0.17.

Petrographic observations in the studied metacarbonate sequence supporting the $H_2O$-rich composition of the metamorphic fluid are: (1) the predominance of titanite over rutile as a stable $TiO_2$-bearing phase (titanite is stable at more water-rich conditions than rutile), although bulk composition may be an important factor controlling this as well; (2) the abundance of epidote group minerals, usually stable at low $X_{CO_2}$ metamorphic conditions (e.g., Deer et al. 1986; Franz and Spear 1983; Castelli 1991; Ferry 1976).

## Concluding remarks

The mineral assemblage titanite-rutile-calcite-quartz-graphite buffers fluid composition and oxygen fugacity in metacarbonate environments. This paragenesis is common in impure calcareous rocks of various metamorphic grades (e.g., Tanner 1976; Frank 1983; Hoschek 1984) and can be employed in the analysis of metacarbonate phase relations as demonstrated in this study of metacarbonate rocks from the Nevado-Filábride Complex. The potential of graphite-carbonate assemblages to buffer $f_{O_2}$ in petrogenetic environments does not appear to be widely recognized. Such assemblages are not uncommon in ultramafic rocks and iron formations where they may prove to be useful indicators of physicochemical conditions.

The *P-T* conditions (9.5 ± 1 kbar and 560 ± 15 °C) inferred here for the Nevado-Filábride Complex are pertinent to the intermediate-pressure metamorphic event that took place in this complex. The inferred pressure conditions agree with those calculated in the nearby metamorphosed evaporite-pelite sequence (Gómez-Pugnaire et al. 1994) and in other lithological units (metabasites) of the complex. However, the highest-pressure conditions reported elsewhere in metabasites and metapelites (≈ 20 kbar) have not been detected in the metacarbonate rocks. Metamorphic conditions calculated here demonstrate that suppositions made by other authors on the lack of intermediate or high-pressure relicts in the Nevado-Filábride Complex metacarbonate rocks, based on conventional petrographical and chemical methods, were not correct (Nijhuis 1964; Voet 1967; Gómez-Pugnaire 1979; Vissers 1981; Martínez-Martínez 1984; Jabaloy 1991).

**Acknowledgements** First results of this work were obtained in 1992–93 during a stay of V.L.S.-V. at IMP-ETH Zürich with a Beca de Intercambio C.S.I.C.-ETH Zürich. V.L.S.-V. and M.T.G.P. also acknowledge financial support from Project I+D AMB93-0535 (DGICYT) and Grupo de Investigación 4019 (Junta de Andalucía). D. Kerrick, G. Skippen and G. Franz are thanked for constructive reviews.

## References

Bakker HE, de Jong K, Helmers H, Biermann C (1989) The geodynamic evolution of the Internal Zone of the Betic Cordilleras (south-east Spain): a model based on structural analysis and geothermobarometry. J Metamorphic Geol 7: 359–381

Balanyá JC, García-Dueñas V (1986) Grandes fallas de contracción y de extensión implicadas en el contacto entre los dominios de Alborán y Sudibérico en el Arco de Gibraltar. Geogaceta 1: 19–21

Ballèvre M, Lagabrielle Y (1994) Garnet in blueschist-facies marbles from the Queyras unit (Western Alps): its occurrence and its significance. Schweiz Mineral Petrogr Mitt 74: 203–212

Berman RG (1990) Mixing properties of Ca-Mg-Fe-Mn garnets. Am Mineral 75: 328–344

Brouwer HA (1926) The structure of the Sierra Nevada. Proc K Ned Akad Wet XXIX: 878–872

Castelli D (1991) Eclogitic metamorphism in carbonate rocks: the example of impure marbles from the Sesia-Lanzo Zone, Italian Western Alps. J Metamorphic Geol 9: 61–77

Chatterjee ND, Froese E (1975) A thermodynamic study of the pseudobinary join muscovite-paragonite in the system $KAlSi_3O_8$-$NaAlSi_3O_8$-$Al_2O_3$-$SiO_2$-$H_2O$. Am Mineral 60: 985–993

Connolly JAD (1990) Multivariable phase diagrams: an algorithm based on generalized thermodynamics. Am J Sci 290: 666–718

Connolly JAD (1995) Phase diagram methods for graphitic rocks and application to the system C-O-H-FeO-$TiO_2$-$SiO_2$. Contrib Mineral Petrol 119: 94–116

Connolly JAD, Memmi I, Trommsdorff V, Franceschelli M, Ricci CA (1994) Forward modelling of microinclusions and fluid evolution in a graphitic metapelite (NE Sardinia). Am Mineral 79: 960–972

Deer WA, Howie RA, Zussman J (1986) Disilicates and ring silicates. (Rock-forming minerals, 1B) Longman, London, pp 2–151.

Enami M, Suzuki K, Liou JG, Bird DK (1993) Al-$Fe^{3+}$ and F-OH substitutions in titanite and constraints on their *P-T* dependence. Eur J Mineral 5: 219–231

Ernst WG (1972) $CO_2$-poor composition of the fluid attending Franciscan and Sanbagawa low-grade metamorphism. Geochim Cosmochim Acta 36: 497–504

Ferry JM (1976) $P$, $T$, $f_{CO_2}$, and $f_{H_2O}$ during metamorphism of calcareous sediments in the Waterville-Vassalboro area, south-central Maine. Contrib Mineral Petrol 57: 119–143

Frank E (1983) Alpine metamorphism of calcareous rocks along a cross-section in the Central Alps: occurrence and breakdown of muscovite, margarite and paragonite. Schweiz Mineral Petrogr Mitt 63: 37–93

Franz G, Selverstone J (1992) An empirical phase diagram for the clinozoisite-zoisite transformation in the system $Ca_2Al_3Si_3O_{12}(OH)$-$Ca_2Al_2Fe^{3+}Si_3O_{12}(OH)$. Am Mineral 77: 631–642

Franz G, Spear FS (1983) High pressure metamorphism of siliceous dolomites from the Central Tauern Window, Austria. Am J Sci 283-A: 396–413

Franz G, Spear FS (1985) Aluminous titanite (sphene) from the eclogite-zone, south-central Tauern Window, Austria. Chem Geol 50: 33–46

Ganguin J (1986) Reliques de faciès éclogitique dans des métasédiments polymétamorphiques: le cas d'un marbre de la couverture des ophiolites de la région de Zermatt, Alpes penniques, Suisse. C R Acad Sci Paris 303, II: 575–580

Ghent ED, Stout MZ (1994) Geobarometry of low-temperature eclogites: applications of isothermal pressure-activity calculations. Contrib Mineral Petrol 116: 500–507

Gómez-Pugnaire MT (1979) La evolución del metamorfismo alpino en el Complejo Nevado-Filábride de la Sierra de Baza (Cordilleras Béticas, España). PhD thesis, Granada Univ, Spain

Gómez-Pugnaire MT, Fernández-Soler JM (1987) High-pressure metamorphism in metabasites from the Betic Cordilleras (SE Spain) and its evolution during the Alpine orogeny. Contrib Mineral Petrol 95: 231–244

Gómez-Pugnaire MT, Franz G, López Sánchez-Vizcaíno V (1994) Retrograde formation of NaCl-scapolite in high-pressure metaevaporites from the Cordilleras Béticas (Spain). Contrib Mineral Petrol 116: 448–461

Hewitt DA (1973) The metamorphism of micaceous limestones from south-central Connecticut. Am J Sci 273A: 444–469

Holland TJB, Powell R (1990) An enlarged and updated internally consistent dataset with uncertainties and correlations: the system $K_2O$-$Na_2O$-CaO-MgO-MnO-FeO-$Fe_2O_3$-$Al_2O_3$-$TiO_2$-$SiO_2$-C- $H_2$-$O_2$. J Metamorphic Geol 8: 89–124

Holloway JR (1977) Fugacity and activity of molecular species in supercritical fluids. In: Fraser D (ed) Thermodynamics in geology. Reidel, Boston, pp 161–181

Hoschek G (1984) Alpine metamorphism of calcareous metasediments in the Western Hohe Tauern, Tyrol: mineral equilibria in COHS fluids. Contrib Mineral Petrol 87: 129–137

Hunt JA, Kerrick DM (1977) The stability of sphene; experimental redetermination and geologic implications. Geochim Cosmochim Acta 41: 279–288

Jabaloy A (1991) La estructura de la región occidental de la Sierra de los Filabres (Cordilleras Béticas). PhD thesis, Granada Univ, Spain

Kerrick DM, Jacobs GK (1981) A modified Redlich-Kwong equation for $H_2O$, $CO_2$ and $H_2O$-$CO_2$ mixtures at elevated temperatures and pressures. Am J Sci 281: 735–767

Korzhinskii DS (1959) Physicochemical basis of the analysis of the paragenesis of minerals. Consult Bur Inc, New York

Kretz R (1983) Symbols for rock-forming minerals. Am Mineral 68: 277–279

Leake BE (1978) Nomenclature of amphiboles. Can Mineral 16: 501–520

López Sánchez-Vizcaíno V (1994) Evolución petrológica y geoquímica de las rocas carbonáticas y litologías asociadas en el área de Macael-Cóbdar (Almería), Complejo Nevado-Filábride, Cordilleras Béticas, SE España. PhD thesis, Granada Univ, Spain

López Sánchez-Vizcaíno V, Franz G, Gómez-Pugnaire MT (1995) The behaviour of Cr during metamorphism of carbonate rocks from the Nevado-Filábride Complex, Betic Cordilleras, Spain. Can Mineral 33: 85–104

Martínez-Martínez JM (1984) Evolución tectono-metamórfica del Complejo Nevado-Filábride en el sector de unión entre Sierra Nevada y Sierra de los Filabres, Cordilleras Béticas (España). Cuad Geol Univ Granada 13

Nesbitt BE, Essene EJ (1983) Metamorphic volatile equilibria in a portion of the southern Blue Ridge Province. Am J Sci 283: 135–165

Newton RC, Charlu TV, Kleppa OJ (1980) Thermochemistry of the high structural state plagioclases. Geochim Cosmochim Acta 44: 933–941

Nijhuis HJ (1964) Plurifacial alpine metamorphism in the south-eastern Sierra de los Filabres, south of Lubrín. PhD thesis, Amsterdam Univ, Netherlands

Puga E, Díaz de Federico A (1976) Metamorfismo polifásico y deformaciones alpinas en el Complejo de Sierra Nevada, implicaciones geodinámicas. In: Reunión sobre la geodinámica de las Cordilleras Béticas y del Mar de Alborán, Granada. pp 79–111

Puga E, Díaz de Federico A, Fediukova E, Bondi M, Morten L (1989) Petrology, geochemistry and metamorphic evolution of the ophiolitic eclogites and related rocks from the Sierra Nevada (Betic Cordilleras, Southeastern Spain). Schweiz Mineral Petrogr Mitt 69: 435–455

Tanner PWG (1976) Progressive regional metamorphism of thin calcareous bands from the Moinian rocks of N.W. Scotland. J Petrol 17: 100–134

Thompson JB (1981) An introduction to the mineralogy and petrology of the biopyriboles. In: Veblen DR (ed) Amphiboles and other hydrous pyriboles-Mineralogy (Reviews in mineralogy, 9A) Mineral Soc Am, Washington, DC, pp 141–188

Vissers RLM (1981) A structural study of the Central Sierra de los Filabres (Betic Zone, SE Spain), with emphasis on deformational processes and their relation to the Alpine metamorphism. GUA Pap Geol Ser 1, 15

Voet HW (1967) Geological investigations in the northern Sierra de los Filabres around Macael and Cóbdar, south-eastern Spain. PhD thesis, Amsterdam Univ, Netherlands